

## **Supplementary Material for manuscript**

### **“Harmful algae and export production collapse in the equatorial Atlantic during the zenith of Middle Eocene Climatic Optimum warmth”**

**Margot J. Cramwinckel<sup>1</sup>, Robin van der Ploeg<sup>1</sup>, Peter K. Bijl<sup>1</sup>, Francien Peterse<sup>1</sup>, Steven M. Bohaty<sup>2</sup>, Ursula Röhl<sup>3</sup>, Stefan Schouten<sup>1,4</sup>, Jack J. Middelburg<sup>1</sup>, Appy Sluijs<sup>1</sup>**

*<sup>1</sup>Department of Earth Sciences, Faculty of Geoscience, Utrecht University, Utrecht, The Netherlands*

*<sup>2</sup>Ocean and Earth Science, National Oceanography Centre Southampton, University of Southampton, Southampton, United Kingdom*

*<sup>3</sup>MARUM Center for Marine Environmental Sciences, University of Bremen, Bremen, Germany*

*<sup>4</sup>NIOZ Royal Netherlands Institute for Sea Research and Utrecht University, Department of Marine Microbiology and Biogeochemistry, Den Burg, Texel, The Netherlands*

## **Contents**

### **1. Supplementary Methods**

### **2. Supplementary Figures**

### **3. Supplementary Tables**

### **4. Supplementary References**

# 1 Supplementary Methods

## 1.1 Palynology

We use the palynological materials from Cramwinckel et al., (2018). Tablets containing a known amount of *Lycopodium clavatum* spores were added prior to palynological processing to allow for quantification of the absolute number of dinocysts per sample. Samples were then treated with 30% HCl and ~38–40% HF and isolation of the 15–250  $\mu\text{m}$  fraction was established using nylon mesh sieves and an ultrasonic bath to break up agglutinated particles of the residue. Palynomorphs were counted up to a minimum of 200 identified dinocysts. Dinocyst taxonomy as cited in (Williams et al., 2017) was followed. Functional ecological dinocyst grouping follows (Brinkhuis, 1994; Sluijs et al., 2005; Frieling and Sluijs, 2018). In particular, the Protoperidinioids, cysts of Protoperidiniaceae, are thought to derive from heterotrophic dinoflagellates and proliferate under increased nutrient conditions (Sluijs et al., 2005). Goniodomids (cf. Sluijs and Brinkhuis, 2009), cysts of Goniodomaceae, including *Polysphaeridium* spp., are considered to be characteristic for restricted, typically lagoonal settings, and can tolerate large swings in salinity (Brinkhuis, 1994; Frieling and Sluijs, 2018). Organic linings of benthic foraminifera were also incorporated into the palynological counts, the presence of which indicates presence of benthic foraminifera.

## 1.2 Core images

For characterization of bioturbation and color changes throughout the MECO interval, high resolution images of Cores 13R–23R (archive halves) were made using a GEOTEK Geoscan-III linescan camera (aperture 6.7 and 8.0) at MARUM, Bremen University. Changes in sedimentary structures were assessed by scoring the types of bioturbation and by measuring the maximum burrow diameter in each section. Burrows were measured from the digital core photos.

Presence of trace fossils in the sediment indicates presence of metazoa living at the seafloor. Food supply is a major factor governing body size of benthic organisms (Danovaro et al., 2014; Rex et al., 2006; Wei et al., 2010). Therefore, burrow size can be used as a qualitative indicator for downward organic carbon fluxes.

## 1.3 Bulk carbonate stable isotope ratios

Stable carbon ( $\delta^{13}\text{C}$ ) and oxygen ( $\delta^{18}\text{O}$ ) isotope ratios of bulk carbonate (40 samples; 0.3–2 mg of freeze-dried and powdered sample) were measured at the Royal Netherlands Institute for Sea Research (NIOZ), using a Thermo Scientific Kiel IV carbonate device coupled to a Thermo Scientific MAT 253 isotope ratio mass spectrometer. Values are reported relative to the Vienna Pee Dee Belemnite (VPDB) standard. Analytical (internal) precision is  $\pm 0.07\text{‰}$  for  $\delta^{13}\text{C}$  and  $\pm 0.1\text{‰}$  for  $\delta^{18}\text{O}$ , supported by NBS-19 and internal laboratory (VICS) standards.

## 1.4 Organic carbon and nitrogen content, organic carbon isotopes

Samples were analyzed for total organic carbon (TOC) and nitrogen contents, as well as the carbon isotopic composition of TOC ( $\delta^{13}\text{C}_{\text{org}}$ ). ~0.3 g of freeze-dried bulk sediment was powdered and decalcified using 1 M

HCl. Samples were dried in a stove at 50°C, and subsequently, TOC and N contents were measured on ~10 mg of powdered, homogenized residue using a CNS analyzer (Fisons). Stable carbon isotope ratios were determined using an isotope ratio mass spectrometer (IRMS; Finnigan DELTAplus) coupled online to the CNS analyzer. Absolute reproducibility, based on international and in-house standards, for TOC and  $\delta^{13}\text{C}_{\text{org}}$  was better than 0.1% and 0.05‰, respectively.

TOC content of the sediment is primarily governed by organic matter flux to the sediment and bottom water oxygen conditions. Both molar C/N ratios and  $\delta^{13}\text{C}_{\text{org}}$  provide indications of organic matter sourcing (*e.g.*, Meyers, 1994).

## 1.5 Bulk sediment elemental composition

Major and minor element composition of the sediment (37 samples) was measured. As the first step in acid digestion, ~125 mg of freeze-dried and powdered sample was dissolved in a mixture of 2.5 mL  $\text{HClO}_4\text{:HNO}_3$  3:2 and 2.5 mL HF (40%) in closed polytetrafluoroethylene autoclaves at 90 °C overnight. Acids were evaporated at 160 °C and the resulting residue was re-dissolved in 25 mL 4.5%  $\text{HNO}_3$  at 90 °C overnight. Elemental compositions of these total acid digested solutions were measured at Utrecht University using Inductively Coupled Plasma-Optical Emission Spectrometry (ICP-OES; Perkin Elmer Optima 3000). Analytical uncertainty was better than 5% based on duplicates and in-house standards. Most of the measured Mo concentrations were below 20 ppm and thus below the background emission line. The error on these measurements can be >10% and values should therefore be regarded as approximates.

Under oxygen-depleted bottom-water conditions, several elements are actively scavenged from the water column into the sediments. Elements such as V, Cr, Cu, Zn, Ni and in particular Mo get enriched in the sediment under such conditions, and their sedimentary contents thus provide a proxy for bottom-water paleo-redox conditions (Brumsack, 1980; Tribovillard et al., 2006; Scott and Lyons, 2012). Detrital elements such as Al, Ti, K and Fe can provide evidence for detrital sediment provenance. Element abundances were assessed in absolute concentrations, but also normalized to Aluminium (Al), in order to correct authigenic enrichment for dilution by the biogenic components of the sediment - here predominantly biogenic silica. Following recommendations by Van der Weijden (2002), regression analysis for normalized elemental values was omitted.

## 1.6 Organic geochemistry

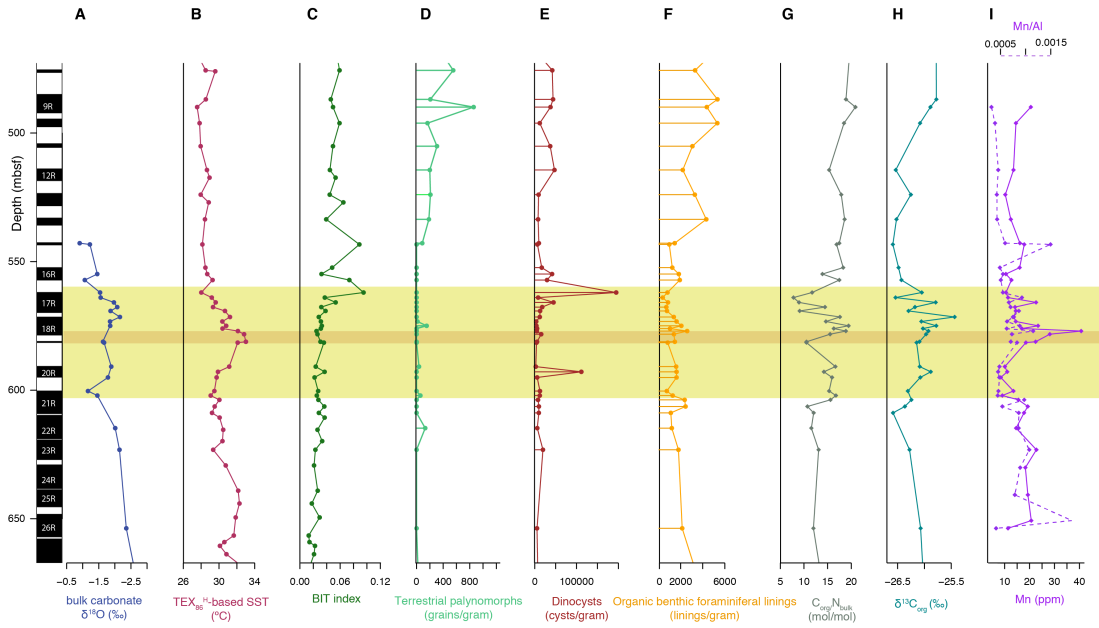
As fully described in Cramwinckel et al. (2018), organic compounds were extracted from Site 959 sediments using an Accelerated Solvent Extractor (ASE) and separated into apolar, polar and neutral fractions using column chromatography. Here, we desulphurized five of the polar fractions across the MECO interval using Raney nickel. These were analysed by gas chromatography-mass spectrometry (GC-MS) at the Royal Netherlands Institute for Sea Research (NIOZ) to assess the presence of isorenieratene and its derivatives.

The compound isorenieratene is a photosynthetic pigment that derives solely from green sulphur bacteria (Overmann et al., 1992). Presence of this biomarker or its derivatives thus indicates development of photic zone euxinia (Sinninghe Damsté et al., 1993), although absence of preserved isorenieratene in the sediment is not evidence of absence of photic zone euxinia.

## 1.7 Stratigraphy

Core recovery in the middle part of the MECO is poor (**Figure 2**). Peak MECO temperatures were recorded in Sections 959D-19R-1 and 959D-18R-5. Recovery of Core 959D-19R is poor (7.6%) and the position of Core 959D-19R relative to -18R and -20R is uncertain, as we were unable to precisely correlate core data from this interval to downhole logging data (Masle et al., 1996). This raises the question whether the recorded MECO warming in available core material underestimates the total warming that occurred at Site 959. Based on the following lines of evidence, we argue that, while the 3.5°C temperature change remains a minimum estimate, it is unlikely a gross underestimate. First, based on the evolution of MECO temperatures as recorded in other sites (Bohaty et al., 2009; Bohaty and Zachos, 2003), peak temperatures are typically reached at the end of the event. As we record similar temperatures in the top of Core 959D-19R and bottom of 959D-18R, it is likely that both of these core intervals represent the interval of peak MECO warming. Our complementary  $\delta^{18}\text{O}$  record (**Figure DR1**) also shows minimum values at the end of the MECO (upper Core 959D-18R), supporting interpreted peak warmth. Secondly, the rapid warming within Core 959D-19R itself also suggests this core interval sampled the peak of the event. Therefore, we argue that our record most likely captures close to the full extent of the SST change, and we can thus make inferences about peak MECO relative to MECO warming and cooling. In this, we refer to the phase of warming based on  $\text{TEX}_{86}$  SST as “MECO warming”, the phase of peak MECO SST as “peak MECO”, and the SST decrease back to pre-MECO SSTs as “MECO recovery”.

## 2 Supplementary Figures





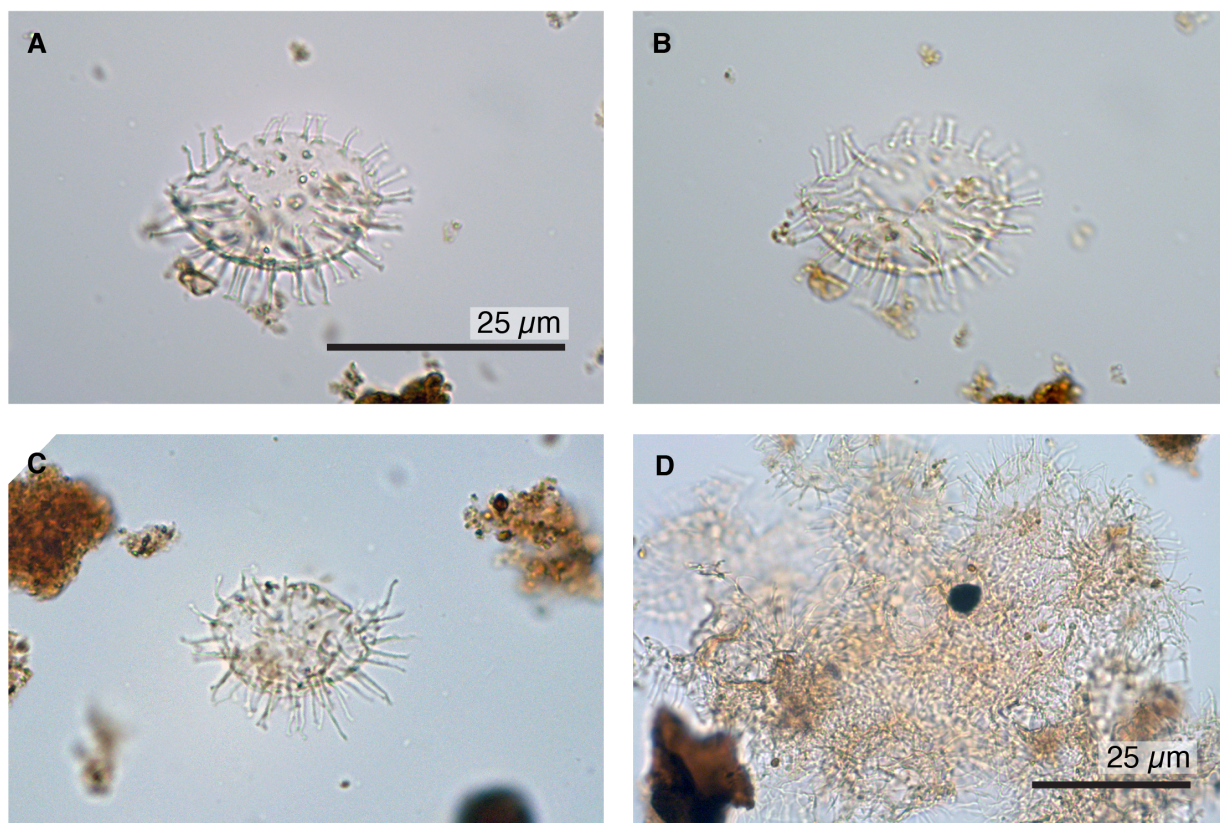




**Figure DR1. Additional geochemical and palynological records of oceanographic and environmental change during the MECO at ODP Site 959.** All against depth in meters below seafloor (mbsf). Plotted with recovery of cores in black. **A.** Oxygen isotopic composition ( $\delta^{18}\text{O}$ ) of bulk carbonate. **B.**  $\text{TEX}_{86}^{\text{H}}$ -based sea surface temperature (SST) reconstruction (Cramwinckel et al., 2018). Yellow shading represents elevated MECO temperatures, with peak MECO temperatures in orange shading. **C.** Branched and Isoprenoid Tetraether (BIT) index. **D.** Absolute quantitative abundances of terrestrial palynomorphs (grains/gram). **E.** Absolute quantitative abundances of dinocysts (cysts/gram). **F.** Absolute quantitative abundances of organic linings of benthic foraminifera (linings/gram). **G.** Molar  $\text{C}_{\text{org}}/\text{N}_{\text{bulk}}$  ratio. **H.** Carbon isotopic composition ( $\delta^{13}\text{C}$ ) of bulk organic material (per mille; ‰). **I.** Manganese (Mn) contents in ppm (solid lines) and normalized to Al (dotted lines).



**Figure DR2.** Light microscope images of the dinocyst *Polysphaeridium zoharyi*. **A, B.** Specimen from 959D-18R-4W, 15-17 cm. **C.** Specimen from 959D-18R-5W, 85-87 cm. **D.** Multiple specimens from 959D-18R-5W, 85-87 cm. Scale bars represent 25 μm. A–C share the same scale.

### 3 Supplementary Tables

**Table DR1.** Presence (black infill) and absence (white infill) of bioturbation types and maximum burrow diameter (mm) present in ODP Hole 959D, core 13R-23R, for all sections longer than 70 cm. The two sections in which the highest MECO SSTs and lowest average burrow diameter (**Figure 2**) were found are outlined in red.

Core	13			14		15	16			17					18					19	20			21						22						23					
Section	1	2	3	1	2	1	1	2	3	1	2	3	4	5	1	2	3	4	5	1	1	2	3	1	2	3	4	5	6	1	2	3	4	5	6	1	2	3	4	5	
 Planolites (<5mm)																																									
 Planolites (>5mm)																																									
 Chondrites																																									
 Thalassinoides																																									
 Zoophycos																																									
 Teichichnus																																									
maximum burrow diameter (mm)	12	8	16	7	13	12	8	9	5	8	6	11	8	14	10	11	12	10	5	2	11	10	5	5	7	9	11	16	10	7	11	14	10	12	14	15	12	9	8	10	

**Table DR2.** Summary of inferred (export) productivity change during the MECO.

Ocean basin	Region	Site / Section	Proxy / Proxies	MECO phase	Signal	Interpretation	References
Atlantic	equatorial	ODP Site 959	TOC%, trace elements, dinocysts, bioturbation	1 (warming)	-	-	this study
				2 (peak warmth)	<i>Polysphaeridium</i> peak, bioturbation size decrease	decreased export productivity	
				3 (recovery)	Redox-sensitive trace element increase, TOC% increase	decreased bottom-water oxygenation, possibly increased export productivity	
Atlantic	northwest	ODP Site 1051	Siliceous microfossils, benthic foraminifera	1	Siliceous microfossil flux increase	increased export productivity	(Witkowski et al., 2014; Moebius et al., 2015)
				2	Siliceous microfossil flux decrease, planktic and benthic foram flux increase	inconsistent	
				3	Siliceous microfossil flux increase, planktic and benthic foram flux increase	increased export productivity	
Atlantic	southeast	ODP Site 1263	Benthic foraminifera	1	Benthic foram flux decrease	decreased export productivity	(Boscolo-Galazzo et al., 2015, 2014)
				2	Benthic foram flux decrease	decreased export productivity	
Tethys	west central	Alano	TOC%, planktic foraminifera, benthic foraminifera, nannofossils	1	Eutrophic benthic and planktonic foram assemblages, nannofossil assemblages somewhat more eutrophic	increased export productivity	(Boscolo-Galazzo et al., 2013; Luciani et al., 2010; Spofforth et al., 2010; Toffanin et al., 2011)
				3	Eutrophic benthic and planktonic foram assemblages, TOC%-rich intervals	even more increased export productivity	
Pacific	southwest	ODP Site 1172	Dinocysts	1–3	Dinocyst P/G ratio decrease	decreased productivity	(Bijl et al., 2010)
Pacific	equatorial	ODP Site 1218	Biogenic silica	1–3(?)	Reduced biogenic silica flux	decreased productivity	(Lyle, 2005)
Indian	equatorial	ODP Site 711	Magnetofossils, biogenic silica	1–3(?)	Bacterially-produced magnetic mineral increase, biogenic silica content increase	increased export productivity	(Savian et al., 2016)
Indian	south	ODP Site 748 & 738	Siliceous microfossils, benthic foraminifera, nannofossils	1	Siliceous microfossil content increase, eutrophic nannofossil assemblage, eutrophic benthic foram assemblage	increased export productivity	(Moebius et al., 2014; Villa et al., 2014, 2008; Witkowski et al., 2012)
				2	Siliceous microfossil content increase, eutrophic benthic foram assemblage	increased export productivity	
				3	Siliceous microfossil content decrease, oligotrophic nannofossil assemblage	decreased productivity	



## 4 Supplementary References

- Bijl, P.K., Houben, A.J.P., Schouten, S., Bohaty, S.M., Sluijs, A., Reichart, G.-J., Damsté, J.S.S., Brinkhuis, H., 2010. Transient Middle Eocene Atmospheric CO<sub>2</sub> and Temperature Variations. *Science* 330, 819–821. <https://doi.org/10.1126/science.1193654>
- 5 Boscolo-Galazzo, F., Giusberti, L., Luciani, V., Thomas, E., 2013. Paleoenvironmental changes during the Middle Eocene Climatic Optimum (MECO) and its aftermath: The benthic foraminiferal record from the Alano section (NE Italy). *Palaeogeogr. Palaeoclimatol. Palaeoecol.* 378, 22–35. <https://doi.org/10.1016/j.palaeo.2013.03.018>
- 10 Boscolo-Galazzo, F., Thomas, E., Giusberti, L., 2015. Benthic foraminiferal response to the Middle Eocene Climatic Optimum (MECO) in the South-Eastern Atlantic (ODP Site 1263). *Palaeogeogr. Palaeoclimatol. Palaeoecol.* 417, 432–444. <https://doi.org/10.1016/j.palaeo.2014.10.004>
- 15 Boscolo-Galazzo, F., Thomas, E., Pagani, M., Warren, C., Luciani, V., Giusberti, L., 2014. The middle Eocene climatic optimum (MECO): A multiproxy record of paleoceanographic changes in the southeast Atlantic (ODP Site 1263, Walvis Ridge). *Paleoceanography* 29, 2014PA002670. <https://doi.org/10.1002/2014PA002670>
- Brinkhuis, H., 1994. Late Eocene to Early Oligocene dinoflagellate cysts from the Priabonian type-area (Northeast Italy): biostratigraphy and paleoenvironmental interpretation. *Palaeogeogr. Palaeoclimatol. Palaeoecol.* 107, 121–163. [https://doi.org/10.1016/0031-0182\(94\)90168-6](https://doi.org/10.1016/0031-0182(94)90168-6)
- 20 Brumsack, H.-J., 1980. Geochemistry of Cretaceous black shales from the Atlantic Ocean (DSDP Legs 11, 14, 36 and 41). *Chem. Geol.* 31, 1–25. [https://doi.org/10.1016/0009-2541\(80\)90064-9](https://doi.org/10.1016/0009-2541(80)90064-9)
- Cramwinckel, M.J., Huber, M., Kocken, I.J., Agnini, C., Bijl, P.K., Bohaty, S.M., Frieling, J., Goldner, A., Hilgen, F.J., Kip, E.L., Peterse, F., Ploeg, R. van der, Röhl, U., Schouten, S., Sluijs, A., 2018. Synchronous tropical and polar temperature evolution in the Eocene. *Nature* 559, 382–386. <https://doi.org/10.1038/s41586-018-0272-2>
- 25 Danovaro, R., Snelgrove, P.V.R., Tyler, P., 2014. Challenging the paradigms of deep-sea ecology. *Trends Ecol. Evol.* 29, 465–475. <https://doi.org/10.1016/j.tree.2014.06.002>
- Frieling, J., Sluijs, A., 2018. Towards quantitative environmental reconstructions from ancient non-analogue microfossil assemblages: Ecological preferences of Paleocene – Eocene dinoflagellates. *Earth-Sci. Rev.* <https://doi.org/10.1016/j.earscirev.2018.08.014>
- 30 Luciani, V., Giusberti, L., Agnini, C., Fornaciari, E., Rio, D., Spofforth, D.J.A., Pälike, H., 2010. Ecological and evolutionary response of Tethyan planktonic foraminifera to the middle Eocene climatic optimum (MECO) from the Alano section (NE Italy). *Palaeogeogr. Palaeoclimatol. Palaeoecol.* 292, 82–95. <https://doi.org/10.1016/j.palaeo.2010.03.029>
- 35 Lyle, 2005. Biogenic sedimentation in the Eocene equatorial Pacific—The stuttering greenhouse and Eocene carbonate compensation depth.
- Meyers, P.A., 1994. Preservation of elemental and isotopic source identification of sedimentary organic matter. *Chem. Geol.* 114, 289–302.
- 40 Moebius, I., Friedrich, O., Edgar, K.M., Sexton, P.F., 2015. Episodes of intensified biological productivity in the subtropical Atlantic Ocean during the termination of the Middle Eocene Climatic Optimum (MECO). *Paleoceanography* 30, 2014PA002673. <https://doi.org/10.1002/2014PA002673>
- 45 Moebius, I., Friedrich, O., Scher, H.D., 2014. Changes in Southern Ocean bottom water environments associated with the Middle Eocene Climatic Optimum (MECO). *Palaeogeogr. Palaeoclimatol. Palaeoecol.* 405, 16–27. <https://doi.org/10.1016/j.palaeo.2014.04.004>
- Overmann, J., Cypionka, H., Pfennig, N., 1992. An extremely low-light adapted phototrophic sulfur bacterium from the Black Sea. *Limnol. Oceanogr.* 37, 150–155. <https://doi.org/10.4319/lo.1992.37.1.0150>
- 50 Rex, M.A., Etter, R.J., Morris, J.S., Crouse, J., McClain, C.R., Johnson, N.A., Stuart, C.T., Deming, J.W., Thies, R., Avery, R., 2006. Global bathymetric patterns of standing stock and body size in the deep-sea benthos. *Mar. Ecol. Prog. Ser.* 317, 1–8.
- Savian, J.F., Jovane, L., Giorgioni, M., Iacoviello, F., Rodelli, D., Roberts, A.P., Chang, L., Florindo, F., Sprovieri, M., 2016. Environmental magnetic implications of magnetofossil occurrence during the Middle Eocene Climatic Optimum (MECO) in pelagic sediments from the equatorial Indian Ocean. *Palaeogeogr. Palaeoclimatol. Palaeoecol., Impact, Volcanism, Global changes and Mass Extinctions* 441, Part 1, 212–222. <https://doi.org/10.1016/j.palaeo.2015.06.029>
- 55 Scott, C., Lyons, T.W., 2012. Contrasting molybdenum cycling and isotopic properties in euxinic versus non-euxinic sediments and sedimentary rocks: Refining the paleoproxies. *Chem. Geol.*
- 60

- Sinninghe Damsté, J.S., Wakeham, S.G., Kohnen, M.E.L., Hayes, J.M., de Leeuw, J.W., 1993. A 6,000-year sedimentary molecular record of chemocline excursions in the Black Sea. *Nature* 362, 827–829. <https://doi.org/10.1038/362827a0>
- 65 Sluijs, A., Brinkhuis, H., 2009. A dynamic climate and ecosystem state during the Paleocene-Eocene Thermal Maximum – inferences from dinoflagellate cyst assemblages at the New Jersey Shelf. *Biogeosciences Discuss* 6, 5163–5215. <https://doi.org/10.5194/bgd-6-5163-2009>
- 70 Sluijs, A., Pross, J., Brinkhuis, H., 2005. From greenhouse to icehouse; organic-walled dinoflagellate cysts as paleoenvironmental indicators in the Paleogene. *Earth-Sci. Rev.* 68, 281–315. <https://doi.org/10.1016/j.earscirev.2004.06.001>
- Spofforth, D.J.A., Agnini, C., Pälike, H., Rio, D., Fornaciari, E., Giusberti, L., Luciani, V., Lanci, L., Muttoni, G., 2010. Organic carbon burial following the middle Eocene climatic optimum in the central western Tethys. *Paleoceanography* 25. <https://doi.org/10.1029/2009PA001738>
- 75 Toffanin, F., Agnini, C., Fornaciari, E., Rio, D., Giusberti, L., Luciani, V., Spofforth, D.J.A., Pälike, H., 2011. Changes in calcareous nannofossil assemblages during the Middle Eocene Climatic Optimum: Clues from the central-western Tethys (Alano section, NE Italy). *Mar. Micropaleontol.* 81, 22–31. <https://doi.org/10.1016/j.marmicro.2011.07.002>
- 80 Tribouvillard, N., Algeo, T.J., Lyons, T., Riboulleau, A., 2006. Trace metals as paleoredox and paleoproductivity proxies: An update. *Chem. Geol.* 232, 12–32. <https://doi.org/10.1016/j.chemgeo.2006.02.012>
- Van der Weijden, C.H., 2002. Pitfalls of normalization of marine geochemical data using a common divisor. *Mar. Geol.* 184, 167–187. [https://doi.org/10.1016/S0025-3227\(01\)00297-3](https://doi.org/10.1016/S0025-3227(01)00297-3)
- 85 Villa, G., Fioroni, C., Pea, L., Bohaty, S., Persico, D., 2008. Middle Eocene–late Oligocene climate variability: Calcareous nannofossil response at Kerguelen Plateau, Site 748. *Mar. Micropaleontol.* 69, 173–192. <https://doi.org/10.1016/j.marmicro.2008.07.006>
- Villa, G., Fioroni, C., Persico, D., Roberts, A.P., Florindo, F., 2014. Middle Eocene to Late Oligocene Antarctic glaciation/deglaciation and Southern Ocean productivity. *Paleoceanography* 29, 2013PA002518. <https://doi.org/10.1002/2013PA002518>
- 90 Wedepohl, K.H., 1971. Environmental influences on the chemical composition of shales and clays. *Phys. Chem. Earth* 8, 307–333. [https://doi.org/10.1016/0079-1946\(71\)90020-6](https://doi.org/10.1016/0079-1946(71)90020-6)
- Wei, C.-L., Rowe, G.T., Escobar-Briones, E., Boetius, A., Soltwedel, T., Caley, M.J., Soliman, Y., Huettmann, F., Qu, F., Yu, Z., Pitcher, C.R., Haedrich, R.L., Wicksten, M.K., Rex, M.A., Baguley, J.G., Sharma, J., Danovaro, R., MacDonald, I.R., Nunnally, C.C., Deming, J.W., 95 Montagna, P., Lévesque, M., Weslawski, J.M., Wlodarska-Kowalczyk, M., Ingole, B.S., Bett, B.J., Billett, D.S.M., Yool, A., Bluhm, B.A., Iken, K., Narayanaswamy, B.E., 2010. Global Patterns and Predictions of Seafloor Biomass Using Random Forests. *PLOS ONE* 5, e15323. <https://doi.org/10.1371/journal.pone.0015323>
- Williams, G.L., Fensome, R.A., MacRae, R.A., 2017. The Lentin and Williams Index of Fossil 100 Dinoflagellates 2017 Edition, AASP Contributions Series.
- Witkowski, J., Bohaty, S.M., Edgar, K.M., Harwood, D.M., 2014. Rapid fluctuations in mid-latitude siliceous plankton production during the Middle Eocene Climatic Optimum (ODP Site 1051, western North Atlantic). *Mar. Micropaleontol.* 106, 110–129. <https://doi.org/10.1016/j.marmicro.2014.01.001>
- 105 Witkowski, J., Bohaty, S.M., McCartney, K., Harwood, D.M., 2012. Enhanced siliceous plankton productivity in response to middle Eocene warming at Southern Ocean ODP Sites 748 and 749. *Palaeogeogr. Palaeoclimatol. Palaeoecol.* 326–328, 78–94. <https://doi.org/10.1016/j.palaeo.2012.02.006>